



Modelling the effect of catena position and hydrology on soil chemical weathering

Vanesa García-Gamero¹, Tom Vanwalleghem¹, Adolfo Peña², Andrea Román-Sánchez³, and Peter A. Finke⁴

¹Department of Agronomy, University of Córdoba, Da Vinci building, Madrid km 396 Rd., 14071 Córdoba, Spain

²Department of Rural Engineering, Civil Constructions and Engineering Projects, University of Córdoba, Da Vinci building, Madrid km 396 Rd., 14071 Córdoba, Spain

³Department of Forest Ecology, Silva Tarouca Research Institute for Landscape and Ornamental Gardening, Lidická 25/27, 602 00 Brno, Czech Republic

⁴Department of Environment, University of Ghent, Coupure Links 653, 9000 Ghent, Belgium

Correspondence: Vanesa García-Gamero (g02gagav@uco.es)

Received: 18 July 2021 – Discussion started: 17 August 2021

Revised: 30 January 2022 – Accepted: 15 February 2022 – Published: 12 April 2022

Abstract. The sensitivity of chemical weathering to climatic and erosional forcing is well established at regional scales. However, soil formation is known to vary strongly along catenas where topography, hydrology, and vegetation cause differences in soil properties and, possibly, chemical weathering. This study applies the SoilGen model to evaluate the link between the topographic position and hydrology with the chemical weathering of soil profiles on a north–south catena in southern Spain.

We simulated soil formation in seven selected locations over a 20 000-year period and compared it against field measurements. There was good agreement between simulated and measured chemical depletion fraction (CDF; $R^2 = 0.47$). An important variation in CDF values along the catena was observed that is better explained by the hydrological variables than by the position along the catena alone or by the slope gradient. A positive trend between CDF data and soil moisture and infiltration and a negative trend with water residence time was found. This implies that these hydrological variables are good predictors of the variability in soil properties.

The model sensitivity was evaluated with a large precipitation gradient (200–1200 mm yr⁻¹). The model results show an increase in the chemical weathering of the profiles up to a mean annual precipitation value of 800 mm yr⁻¹, after which it drops again. A marked depth gradient was obtained for CDF up to 800 mm yr⁻¹, and a uniform depth distribution was obtained with precipitation above this threshold. This threshold reflects a change in behaviour, where the higher soil moisture and infiltration lead to shorter water transit times and decreased weathering. Interestingly, this corroborates similar findings on the relation of other soil properties to precipitation and should be explored in further research.

1 Introduction

The spatial variability in soil properties is conditioned by the following five main soil-forming factors: climate, organisms, relief, parent material, and time (Jenny, 1941). Differences in the spatial and temporal distribution of these factors cause both long- and short-scale spatial heterogeneity. In recent

years, different soil formation models have been developed that explain the landscape or large-scale soil variability well. Such models range from simple mechanistic soil depth models (Minasny and McBratney, 2001) to more complex models that link different soil-forming processes and erosion–deposition, for example, MILES^D or LORICA (Temme and Vanwalleghem, 2016; Vanwalleghem et al., 2013).

However, the short-scale variability, or catena effect, has received much less attention. The interlocking of specific soil and vegetation associations at different landscape positions was first described by Milne (1935) and is widely used in soil science (Borden et al., 2020). The soil catena can be understood from the retention and movement of water and chemical elements linked to topography and vegetation (Reuter and Bell, 2001). Recently, Ferrier and Perron (2020) constructed a numerical model for the coevolution of topography, soils, and soil mineralogy that allowed them to conclude that the hillslope scale has a critical importance in the response of chemical weathering rates to changes in tectonics and climate. However, most existing soil formation models do not account for hydrology, nor for chemical weathering reactions. For example, the models mARM3D (matrices ARMOUR 3D; Cohen et al., 2010) and State Space Soil Production and Assessment Model (SSSPAM; Welivitiya et al., 2019) linked landscape and pedogenesis processes for catena spatial scales, but while they represent physical weathering and armouring well, they did not account for chemical weathering. At present, the only models of soil genesis with the capability of simulating water flow, physical and chemical weathering, and chemical equilibria are one-dimensional, for example, SoilGen (Opolot et al., 2015). In spite of this limitation, such models have been applied successfully at the landscape scale, by modelling the different landscape positions independently. Finke (2012) for example modelled three soil profiles on different topographic positions in the loess belt of Belgium. Finke et al. (2013) modelled the spatial variation in soil horizons at 108 locations in a 1329 ha forest area in the same loess belt region. However, there is still need to further test these one-dimensional models against field data from different environments and, especially, to test their capabilities to model chemical weathering.

Field studies have shown the importance of chemical weathering in the overall soil formation processes and have shown that physical erosion and chemical weathering are tightly coupled (Riebe et al., 2004) as the main processes in eroding environments. The combination of these processes determines the total denudation rate (Riebe et al., 2001). The contribution of chemical weathering (W) to the total denudation rate (D), W/D , can be inferred by comparing the concentration of immobile elements in soil and bedrock, through the chemical depletion fraction (CDF; Riebe et al., 2001).

There is an ongoing debate in the scientific community as to whether chemical weathering is limited by physical erosion and the supply of fresh particles (e.g. Larsen et al., 2014) or whether it is limited by reaction kinetics (e.g. Gabet and Mudd, 2009). Generally, it is assumed from models and field studies in different environments that soil weathering is supply limited when erosion rates are low and kinetically limited when erosion rates increase, as the shorter soil residence times imply that minerals do not stay in the soil long enough to become fully weathered. Larsen et al. (2014) compiled data from the New Zealand Alps, among the world's most

rapidly eroding mountain areas, and still found a positive relation between physical erosion rates and chemical weathering, indicating supply-limited conditions. On the other hand, it is well established that climate and, specifically, water availability are also important factors affecting chemical weathering rates (e.g. Maher, 2011). Climatic factors affect these rates significantly because of the dependency on the chemical weathering types of water to drive the chemical alteration of rocks, and these rates are potentially accelerated by high temperatures because they affect the reaction kinetics and solubilities (Duarte et al., 2017). Schoonejans et al. (2016) confirmed the significant relation of chemical weathering to rainfall by measuring CDF along a climatic gradient in a semiarid environment in the southern Betic cordillera (Spain). Whereas much of soil weathering research has focused on the critical control of physical erosion rates on chemical weathering, more recent research by Calabrese and Porporato (2020) stresses the importance of wetness. They suggest that water-limited environments are kinetically limited. Globally, they calculate 61 % of the land to be kinetically limited, while only 1 % would be supply limited. If their findings can be confirmed, then it would imply that climatic conditions and soil hydrology are much more important than previously assumed. In any case, these authors point out that the factors affecting chemical weathering need to further be disentangled (Calabrese and Porporato, 2020).

However, the relation between weathering and water availability is not limited to precipitation and evapotranspiration but is also related to other factors such as infiltration or topography and even vegetation. Along a catena, the hydrology is considerably different, depending on the position (Chadwick et al., 2013). Dahlgren et al. (1997), in their work developed along an elevational transect in Sierra Nevada in California (USA), found the maximum degree of chemical weathering with intermediate levels of precipitation and temperature. Riebe et al. (2004) made measurements on 42 study sites with highly variable climate regimes, and they showed that the degree of chemical depletion increases systematically with temperature and precipitation. Mudd and Furbish (2006) presented a hillslope model that couples the evolution of topography and soil thickness by using immobile minerals and assessing the importance of hydrology on the rate of chemical weathering in hillslope soils. Yoo et al. (2007) developed a model that integrated the Riebe et al. (2001) method and tested it with experimental data from a watershed in southeastern Australia to simultaneously quantify the rates of chemical weathering and soil transport as a function of hillslope position. Afterward, this work was expanded by Yoo et al. (2009), who quantified soil chemical weathering rates along a grass-covered hillslope in the Tennessee Valley in coastal California (USA) and began to elucidate the mechanisms that control the topographical dependence on chemical weathering, with the next step being the inclusion of hydrology into the model. Samouëlian and Cornu (2008) pointed out the role of water in soil forma-

tion and how the soil moisture regime variation and its influence on soil formation processes were not included in several models. Indeed, the soil moisture dynamics related to the topographical position have been studied by several authors, such as Salve et al. (2012), who have monitored this and other variables for 4 years with multiple measurement devices on a hillslope in coastal Mendocino County, in northern California, USA. Langston et al. (2011) explored the role of hydrology in saprolite formation through 2-D numerical calculations on two idealized slopes, a north-facing slope (NFS) and a south-facing slope (SFS), respectively, in the Boulder Creek watershed, Colorado (USA). This highlighted the importance of time and the hillslope aspect in the formation of the saprolite and the need to couple hydrologic models with reactive transport models to better understand the distribution of chemical weathering intensity. Dixon et al. (2016), along 60 km of a north–south toposequence in the Waitaki valley in the South Island of New Zealand, which is marked with an important precipitation gradient, identified a pedogenic threshold at mean annual precipitation of $\sim 800 \text{ mm yr}^{-1}$. Braun et al. (2016) presented a model for the formation of regolith on geological timescales by chemical weathering, pointing out that this process has long been neglected in favour of the hillslopes' physical processes by geomorphologists because this process is also the mechanism that leads to the formation of aquifers from the unweathered bedrock (Lachassagne and Wyns, 2011). Brantley et al. (2017) developed a conceptual model to link chemical weathering reaction fronts to hillslope hydrology. Knowing how difficult it is for hydrologists to select models, they developed a conceptual model to relate reaction fronts with water flow inside hillslopes, which was exemplified with field data for shale, granite, and diabase. The linear hill, with two layers of lateral water flow, is assumed to be characterized by reaction fronts. The upper and lower reaction fronts are separated by metres beneath the hills on felsic rocks because of weathering-induced fracturing that permits water infiltration to increase the regolith and reaction front thickness and front spacing. In particular, groundwater removes highly soluble minerals, whereas interflow removes moderately soluble minerals. Previously, the weathering zone had been considered the one located over the groundwater level. However, Lebedeva and Brantley (2020) formulated a simplified weathering model to explore relationships between weathering and the water table, taking into account the unsaturated and the saturated zone.

In response to the need to couple hydrology with chemical weathering to understand spatial variability in soil formation, this study applied the SoilGen model (Finke and Hutson, 2008) to different pedons and different hydrological conditions along a catena in a Mediterranean catchment in southern Spain. Finke and Hutson (2008) created the SoilGen model to reconstruct soil development based on present knowledge. It is a 1-D solute transport extended with various soil development processes, such as physical and chemical

weathering, clay migration, and cycles of various elements, including that of C and bioturbation, where soil-forming factors (climate, organisms, relief, parent material, and time) serve as initial and boundary conditions to recreate soil formation over various parent materials.

The specific objectives of this study were (i) to evaluate the differences in simulated soil development between two opposing, north–south-facing hillslopes from 20 000 years before the present to the present, (ii) to relate soil development to differences in hydrological dynamics, and (iii) to evaluate, through sensitivity analysis, the capability of the SoilGen model to simulate soil development in a Mediterranean catchment in granitic parent material.

2 Materials and methods

2.1 SoilGen model

SoilGen (Finke, 2012; Finke and Hutson, 2008) simulates the change in soil properties as a function of properties of the parent material and time-dependent drivers at the soil boundary (climate, vegetation, bioturbation, relief, and deposition or erosion). The model operates at a typical spatial scale of 1 m^2 and covers millennia but takes dynamic time steps that vary per process (Fig. 1), depending on the processing speed. The flow of water, heat, gas, and solutes is represented by numerical solutions to partial differential equations (Richards equation, heat flow equation, gas diffusion equation, and solute advection/dispersion equation), where soil profiles have 5 cm compartments. For water flow, the relationship between the pressure head, water content, and hydraulic conductivity are dynamically parameterized using a pedotransfer function based on the texture, organic matter content, and bulk density. These properties are dynamically simulated per compartment. (i) The fate of organic carbon is simulated according to the concepts of the RothC-26.3 model (Coleman and Jenkinson, 1996), (ii) the texture changes are due to the physical weathering of minerals, (iii) clay migration and bioturbation affect the vertical distribution of all soil components, and (iv) the bulk density varies because of mass gains/losses over the compartment.

Chemical weathering of minerals and organic matter decomposition release ions in the soil solution. These ions are distributed over precipitated, solution, and exchange phases using a Gapon exchange mechanism and chemical equilibria. The model can simulate several agricultural practices and can also accommodate the removal (or addition) of top layers by erosion (or sedimentation, such as dust addition).

2.2 Study site

The study site is located in a semi-natural area of oak woodland savanna or “dehesa” (a traditional Mediterranean silvopastoral system; Olea and San Miguel-Ayanz, 2006) in Cardeña, within the Sierra Morena mountain range, in south-

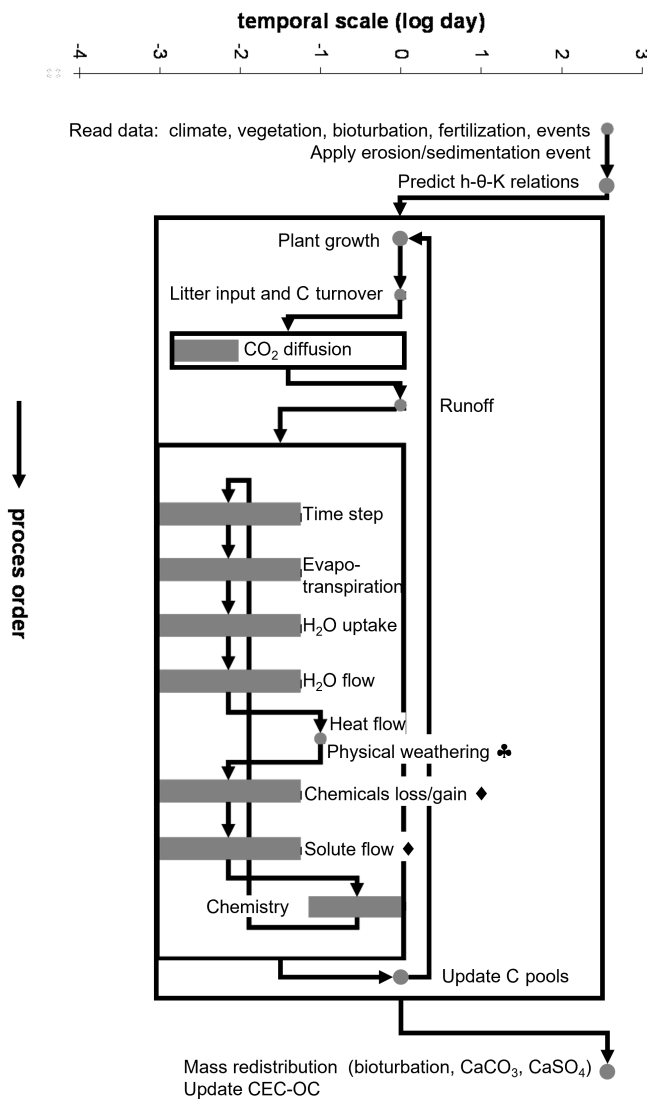


Figure 1. Process flowchart of SoilGen. This figure was published in *Quaternary International*, 265, Peter A. Finke, Modelling the genesis of Luvisols as a function of topographic position in loess parent material, 3–17, Copyright Elsevier (2012).

ern Spain (38.20° N, 4.17° W; 700 m a.m.s.l. (above mean sea level; Fig. 2). The direction of the prevailing winds is southwesterly. A total of seven locations were chosen along a north–south catena, each separated at a distance between 50 and 100 m, on two opposite hillslopes. A summary of the characteristics of the locations is given in Table 1. A full soil profile description was made at each point, and soil samples were taken for chemical analysis up till the bedrock (see the soil profile description in Tables S1–S7 and the physical–chemical characteristics in Table S8 in the Supplement). Next, five soil moisture sensors were installed in each profile at different depths between 5 and 45 cm. For details on the soil hydrology dynamics, see García-Gamero et al. (2021), who studied the interaction between hydrology,

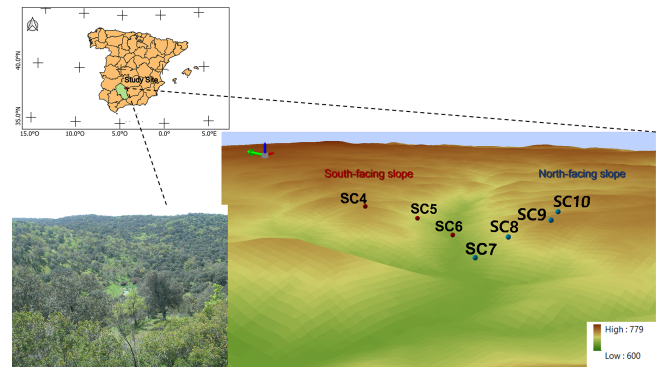


Figure 2. General location map of the study area and a detailed terrain map showing the location of the seven analysed soil profiles along the catena, with two opposing north–south facing slopes (respectively, NFS and SFS; blue and red dots). The inset shows a landscape view of the study area. Note that the green arrow indicates the north.

terrain, and vegetation through soil moisture, vegetation, and water table dynamics measurement, to quantify the aspect influence on ecohydrological dynamics of an oak-woodland savanna or dehesa on two opposing hillslopes of a semi-arid, Mediterranean catchment in southern Spain.

According to the Köppen–Geiger climate classification (Peel et al., 2007), the area has a continental Mediterranean climate (BSk) with an average annual rainfall of 878 mm (1981–2010), with cold winters and long, dry summers. The mean annual air temperature is 15.3 °C, the coldest month is January, with a mean monthly temperature of 7 °C, and the hottest month is July, with a mean monthly temperature of 25.4 °C (Carpintero et al., 2020).

Soils in the catchment are derived from Los Pedroches batholith parent material, which consists of a main granodioritic unit, several granite plutons, and an important acid-to-basic dike complex (Carracedo et al., 2009). These fall into the following three classifications: Regosols, Leptosols, and Cambisols, according to the FAO–Unesco World Reference Base (IUSS Working Group WRB, 2015). The texture class ranges from sand to sandy loam, with a soil depth generally ranging between 0.5 m along the southern aspect part of the transect and 1.0 m along the northern part of the transect (Román-Sánchez et al., 2018), according to soil observations.

Vegetation in a dehesa includes sparse trees, holm (*Quercus ilex* L.) and cork oaks (*Quercus suber*), shrubs, retama, and annual grasses such as *Lolium* sp., *Bromus* sp., and *Trifolium* sp., with maximum production in spring and a non-vegetative period in summer (Olea and San Miguel-Ayanz, 2006).

Table 1. Characteristics of the seven locations (SC4–SC10) in the study site.

	SC4	SC5	SC6	SC7	SC8	SC9	SC10
Landform types*	Summit	Back slope	Toe slope	Toe slope	Back slope	Shoulder	Summit
Slope (°)	4	20	14	4	27	19	2
Upslope bearing (°)	35	27	40	55	61	66	53
Profile curvature (m ⁻¹)	-0.47	-0.22	2.5	1.0	-3.0	0.23	-0.75
Plan curvature (m ⁻¹)	0.78	0.73	-0.39	-0.9	4.24	0.67	-0.65

* Following Schaetzl and Anderson (2005).

2.3 Testing of modelled soil hydrology

SoilGen simulates, over millennial scales, the flow of water, heat, solutes, and CO₂ in unconsolidated geomaterials by numerically solving partial differential equations (the Richards equation, heat flow equation, advection–dispersion equation, and CO₂ diffusion equation, respectively; Finke and Hutson, 2008).

Given the importance of water fluxes for soil formation in general and chemical weathering specifically, the model was tested for its ability to simulate the soil moisture dynamics accurately. For this, the current soil profile characteristics in seven locations were used to run the model over a 2-year period in which soil moisture was measured, i.e., 2016 and 2017. The soil moisture sensors, which are transmission line oscillator probes (model CS655; Campbell Scientific, Inc., Logan, UT), started to collect data at the end of 2016. So, for the first part of the year, the simulations were adapted using precipitation and evapotranspiration data from 2017. This could be considered a spin-up (because the initial soil moisture profile was not known).

To account for interception by vegetation, we reduced the daily precipitation by a fixed value of 2 mm, as suggested by Laio et al. (2001). These changes resulted in a reduction of 718.68 to 525.40 mm in the measured precipitation during the calibration period.

Model-to-data correspondence was tested by comparing simulated values with measured values of soil moisture content by the R^2 and the Nash–Sutcliffe efficiency (NSE).

2.4 Model inputs

The tested model was then run at the seven soil profile location for long-term simulations (20 000 years). This simulation period represents the residence time of the soil profile based on field measurements with optically stimulated luminescence (Román-Sánchez et al., 2019). Table 2 summarizes the main model parameters and initial values. Figure 3 depicts the temporal variation in boundary inputs if the time series were reconstructed over the simulation period. In order to represent the Mediterranean climate variability correctly, the climate data reconstructions were obtained by combining a mean temperature, precipitation, or evapotranspiration

from the pollen-based dataset by Davis et al. (2003), with the observed year-to-year variability in modern weather observations.

2.5 Chemical composition and weathering

The chemical depletion fraction (CDF), expressing the total fractional mass lost to chemical weathering, is a widely used indicator of the degree of chemical weathering of a soil profile, as in the following (Dixon et al., 2009; Riebe et al., 2001):

$$\text{CDF} = 1 - \frac{Zr^{\text{ROCK}}}{Zr^{\text{SOIL}}},$$

where Zr^{ROCK} is the Zr concentration in the bedrock, and Zr^{SOIL} is the Zr concentration in the soil. CDF values close to zero indicate the absence of weathering, as the Zr concentration of the soil is equal to that of the parent material. Values closer to 1 indicate higher chemical weathering, as the weathering of mobile elements results in a relative increase of the immobile Zr in the soil profile (Yoo et al., 2011).

CDF values were measured in the field by sampling each soil profile and comparing it to the minimum value registered in the soil profile (Table 3). The chemical analyses were performed on a Philips model (PW 2404) wavelength-based X-ray fluorescence spectrometer (WDS) with a 4 kW rhodium anode tube. The determination of the major elements was carried out from a fusion bead, with lithium tetraborate and a flux / sample ratio of 10 : 1. Before fusion, the loss on ignition (LOI) was determined by calcining the sample at 975 °C for 2 h. International standards from different geological services have been used for the elaboration of the different calibration lines. For the determination of trace elements, the Pro-Trace programme of the PANalytical company was used, based on calibration curves that include both geological patterns and reference patterns of the programme itself. The samples were prepared in a tablet pressed at 40 t for 2 min. The amount of sample used was 10 g mixed with a solution of Elvacite, with a proportion of 10 g of sample with 4 mL of solution.

The SoilGen model was then used to model the measured CDF values, assuming one completely inert (zero-weathering rate) mineral, and to explore the sensitivity of the

Table 2. Inputs for the SoilGen model. Note: DEM is the digital elevation model, and n and m are the charges of the ion pair involved.

Group	Input variable or parameter	Dimensions	As initial condition	Time series in a typical year	Time series (annual)	Source for data and/or method
Climate	Temperature	° C	Yes	Weekly average and daily amplitude	January and July averages	Davis et al. (2003); Cardaña weather data
	Precipitation	mm	–	Daily depth, intensity, and chemical composition of rain	Annual sum	Davis et al. (2003); Cardaña weather data
Organisms	Potential evapotranspiration	mm	–	Weekly total	Annual sum	Hargreaves and Samani (1985)
	Vegetation type	–	–	–	Vegetation type, rooting depth, and C input as litter	Olea and San Miguel-Ayanz (2006); unpublished data from Santa Clotilde dehesa
Relief	Bioturbation	Mg ha ⁻¹ yr ⁻¹	–	–	Yearly depth distribution	Gobat et al. (1998, p. 122)
	Slope angle	°	Yes	–	–	DEM (García-Gamero et al., 2021)
	Slope aspect	°	Yes	–	–	DEM (García-Gamero et al., 2021)
Parent material	Wind direction	°	Yes	–	–	Cardaña weather data
	Clay/silt/sand	Mass %	Yes	–	–	Granite (7.0/17.4/75.6); unpublished data from analysed horizons in Santa Clotilde dehesa
	OC	Mass %	Yes	–	–	0.17 %
	Ca, Mg, Na, K, Al, SO ₄ , Cl, alkalinity in solution	mmol dm ⁻³	Yes	–	–	Unpublished data
Ca, Mg, Na, K, Al, H on exchange complex and CEC	Ca, Mg, Na, K, Al, H on exchange complex and CEC	mmol + kg ⁻¹	Yes	–	–	Unpublished data from analysed horizons in Santa Clotilde dehesa
	CaCO ₃ / CaSO ₄	Mass %	Yes	–	–	0.01 / 0 %
Gapon exchange coefficients	Gapon exchange coefficients	(mol dm ⁻³) ^{1/n-1} / m	Yes	–	–	Unpublished data from analysed horizons in Santa Clotilde dehesa
	Ca, Mg, Na, K, Al in primary minerals	mol ⁺ kg ⁻¹	Yes	–	–	De Vries and Posch (2003)
Unpublished data from Santa Clotilde dehesa	Ca, Mg, Na, K, Al in primary minerals	mol ⁺ kg ⁻¹	Yes	–	–	Unpublished data from Santa Clotilde dehesa

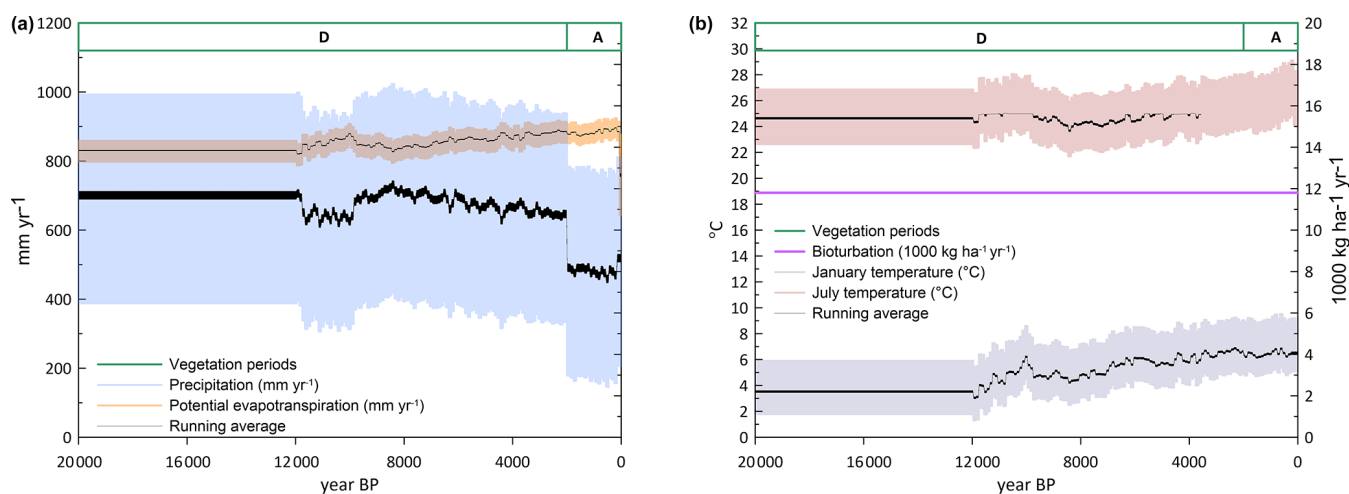


Figure 3. Boundary conditions for the soil modelling, representing reconstructed climate and vegetation change over the last 20 000 years. The left panel shows precipitation and evapotranspiration, and the right panel shows temperature. The bandwidth indicates the year-to-year variability in the climate data, and the bold, black line indicates the 25-year running average. Note: A – agriculture; D – deciduous wood.

Table 3. Chemical composition of the seven soil profiles (SC4–SC7). Values are averaged over the total soil profile depth. The mean measured chemical depletion fraction is indicated as CDF. Note: ppm is parts per million.

Location	Soil profile depth (m)	SiO ₂	Al ₂ O ₃	Fe ₂ O ₃	MnO	MgO (%)	CaO	Na ₂ O	K ₂ O	TiO ₂	P ₂ O ₅	LOI	Zr (ppm)	CDF
SC4	0.44	70.8	16.5	2.3	0.03	1.1	0.56	2.6	4.4	0.40	0.12	0.75	148.0	0.19
SC5	0.60	66.7	17.0	5.1	0.06	1.7	0.28	2.2	4.6	0.83	0.11	1.0	284.9	0.04
SC6	0.55	68.0	16.8	3.9	0.07	1.2	0.27	1.9	5.3	0.69	0.11	1.4	314.2	0.13
SC7	0.97	69.8	16.5	2.6	0.07	1.1	0.46	2.9	4.4	0.48	0.11	1.1	181.3	0.26
SC8	0.47	62.2	18.7	5.7	0.11	3.1	0.51	1.6	4.7	1.03	0.15	1.7	294.0	0.20
SC9	0.57	69.1	17.1	2.8	0.05	1.3	0.45	2.9	4.2	0.48	0.11	1.2	166.6	0.19
SC10	0.51	69.9	16.6	2.7	0.03	1.1	0.61	3.3	4.0	0.46	0.15	1.1	160.6	0.19

CDF to variations in precipitation. The effect on the model results of a marked gradient of precipitation, between 200 and 1200 mm, has been evaluated at the SC10 location because of its position at the summit, which is representative of the larger plateau area.

We conducted the performance evaluation by selecting various statistical indicators to conduct a quantitative analysis, namely the fraction of predictions within a factor of 2 (FAC2), the fractional bias (FB), the root mean square error (RMSE), and the normalized mean square error (NMSE).

X-Ray diffraction (XRD) analysis was performed along the catena to determine the bulk mineralogy. Analyses were conducted using a Bruker D8 ADVANCE instrument, using Cu K α radiation. Samples were ground to a fine powder ($\sim 50\ \mu\text{m}$) and analysed at a rotational speed of $1.116^\circ 2\theta\ \text{min}^{-1}$. X-rays were generated at a setting of 40 kV and 40 mA through a range of $3\text{--}70^\circ (2\theta)$. Peak data for each sample were analysed using DIFFRAC.EVA software and compared to Whittig and Allardice (1986) to determine the mineralogy of the sample.

3 Results and discussion

3.1 Model testing and results

The model was tested using in situ soil moisture observations, in order to check that the model represents the soil profile's hydrological balance before modelling chemical weathering reactions and material fluxes well. The model was adjusted for rainfall interception by vegetation. Figure 4 shows the R^2 values, with the best correlation determined by the daily precipitation reduced by a fixed value of 2 mm and interception evaporation fraction of 0. Consequently, all further simulations were carried out using this combination. The results are shown in Fig. 5, which compares the daily values of simulated and measured soil moisture content across a period of 1 year and 1 month (from November 2016 to December 2017) at the SC4 location, which is at the summit of the SFS. Soil moisture values, both measured and simulated, vary between approximately $0.05\ (\text{m}^3\ \text{m}^{-3})$ and $0.30\ (\text{m}^3\ \text{m}^{-3})$. The calibrated coefficient of determination

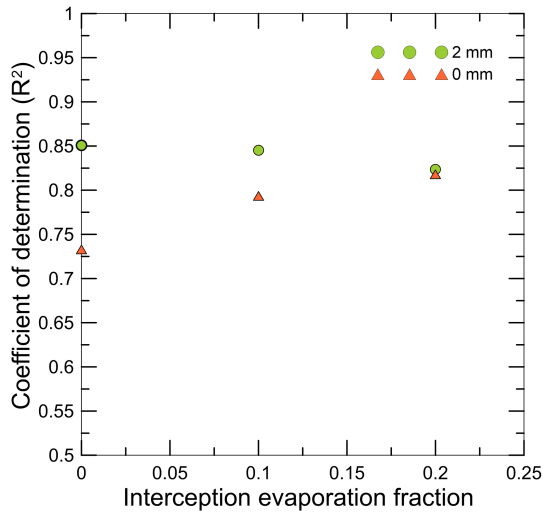


Figure 4. The coefficient of determination (R^2) calculated for different interception evaporation fractions, with the daily precipitation reduced by a fixed value of 2 mm and without reduction (or 0 mm).

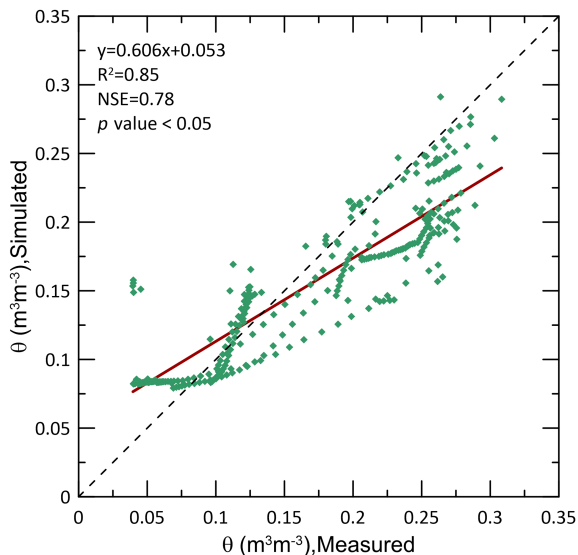


Figure 5. Relation between soil moisture content (θ) values simulated and measured at SC4 location. The coefficient of determination (R^2) and the Nash–Sutcliffe efficiency (NSE) index are indicated.

(R^2) and the Nash–Sutcliffe efficiency (NSE) index indicate a good fit of SoilGen to the observations, with values of 0.85 and 0.78, respectively. Overall, most values fall close to the 1 : 1 line, although there is a small overprediction of low soil moisture values and an underprediction of high soil moisture values. However, given the complex soil conditions and variable Mediterranean climate, this prediction can be considered a valid representation of the actual soil hydrological dynamics.

A comparison between measured and modelled CDF values is shown in Fig. 6. Measured CDF values indicate an intermediate weathering of the soil profiles, with values ranging between 0.04 and 0.26. The highest chemical weathering was measured in the profiles SC7 and SC8 on the NFS. Simulations with SoilGen generally represent the trend in the measured data well, although the data show an overall trend for CDF to be overpredicted (Fig. 6), as the average slope of the regression line ($\text{CDF}_{\text{measured}} = 0.630 \cdot \text{CDF}_{\text{calculated}} + 0.011$) is lower than 1. The 1 : 1 solid line (perfect model) and the 1 : 0.5 and 1 : 2 dashed lines (FAC2) were added to the scatterplot (Fig. 6) to assist the interpretation of the results. The results of the statistical metrics that are used for the quantitative evaluation of the results met the criteria suggested by Kumar et al. (1993) and were also adopted by other authors such as Kontos et al. (2021) or Boylan and Russell (2006). The performance of a model can be deemed as acceptable if $\text{FAC2} \geq 0.80$, with the ideal value being 1.0 (100%), $\text{NMSE} \leq 0.5$, and $-0.5 \leq \text{FB} \leq +0.5$. Taking this into account, the obtained FAC2, NMSE, and FB values are quite acceptable and equal to 0.86, 0.22, and -0.39 , respectively. According to the FAC2 value, 86 % of simulated values were within a factor of 2 of the measured values. A negative value of FB indicates model overestimation, whereas RMSE and NMSE do not account for over- or underestimation, but their ideal value is zero (Brancher et al., 2020). The model, therefore, represents the measured trend in the CDF values correctly, although there exists a positive bias. However, given the fact that the model is uncalibrated in terms of chemical reactions and with respect to the resulting soil properties, we consider this result to be satisfactory. Indeed, some degree of bias can be expected, in part since this 1-D model is not set up to handle possible lateral fluxes of water and chemical weathering products but also because of the large timescale of the modelled processes, which is a common problem in this type of soil formation study (Opolot and Finke, 2015).

The low CDF at the SC5 location, considering the minimum Zr value measured in the soil profile, indicates that the complete soil profile is slightly weathered. This is associated with lower SiO_2 and higher MgO values with respect to the other locations (Table 3). Also, the XRD results (Table 4) indicate localized differences in bedrock mineral composition at this location. The dominant minerals in the catena are quartz, feldspars, and other phyllosilicates such as mica. Kaolinite and chlorite–vermiculite intergrade are accessories. However, the SC5 rock samples differ from the rest of the catena by a lower amount of mica, lower quartz content, and higher chlorite–vermiculite content, which seems to support the results of the chemical composition analysis of Table 3. Further evidence corroborating the different rock composition at the SC5 site, and its consideration as an outlier, is given by the surface topography, as shown in Fig. 7. It can be seen that a small knickpoint is present just upslope of SC5, which could indicate indeed a lower weatherability

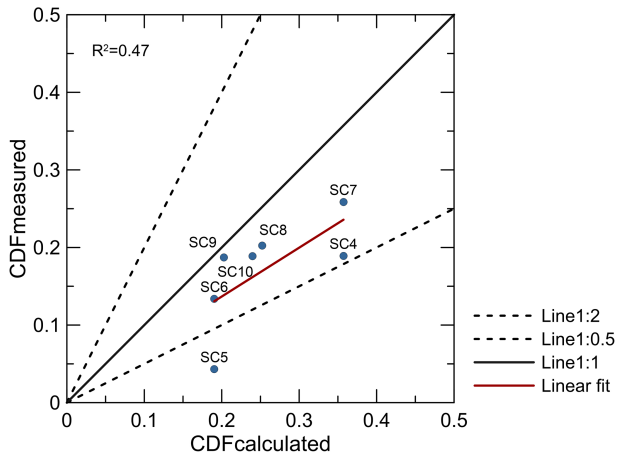


Figure 6. Relation between CDF values calculated based on simulations and measured based on field samples. The 1 : 1 line (solid) represents the perfect model, and the 1 : 0.5 and 1 : 2 lines (dashed) embrace the data within a factor of 2 (FAC2). The coefficient of determination (R^2) is indicated.

around SC5. Also, the SC8 location is characterized by lower SiO₂ and high MgO values, and different mineral composition. However, the simulated CDF at this location does not deviate as much from the measured values as in SC5. This location on the NFS shows denser vegetation than the location of SC5 on the SFS (Fig. 7) due to the higher water availability on the NFS (García-Gamero et al., 2021). This could increase the acid supply and promote weathering at the SC8 location. The effect of vegetation is certainly complex, as other authors such as Oeser and von Blanckenburg (2020) pointed out that the presence of denser vegetation might counteract a potential weathering increase in their study along the climate and vegetation gradient in the Chilean coastal cordillera. They attribute this to an increased nutrient cycling, resulting in an absence of a correlation between CDF and mean annual precipitation in their study. Dong et al. (2019) pointed to complex ecohydrological and soil thickness feedbacks to help understand weathering in karst landscapes, which they found to be highest at intermediate soil depths.

This could explain why SC8 is not an outlier, similar to SC5. While the underlying reasons for any deviations between modelled and measured CDF values are certainly complex, they will be explored below in more detail, in order to try to establish systematic relations between CDF and topographic and hydrological variables.

3.2 Topographic and hydrological effect in CDF

The SoilGen model was applied to test the hypothesis that CDF values could be explained by landscape position and simulated by a simple one-dimensional model. Any deviations can then be analysed to identify model shortcomings and future needs for model improvement.

To analyse the effect of topographic position along the catena, measured and simulated CDF values, together with the conceptual model of the subsurface of the Critical Zone (the zone of the Earth's surface that extends from the top of the canopy to the bottom of the groundwater) in the study site, are shown in Fig. 7. As mentioned in Fig. 6, simulated and measured CDF values generally have the same trend, except for SC5. Higher simulated values were observed on the summit, SC4, and the toe slope, SC7, followed by location SC8 on the back slope of the NFS (Fig. 7). These locations were among those with the lowest local slope gradient, except for SC8.

The position along the toposequence alone did not explain the spatial variation in the CDF well, so it has to be concluded that its variation is due to other factors that are considered in the model and will be analysed below.

The relation of CDF values with different external factors was considered in Fig. 8. The variation in CDF along the toposequence was related to local slope gradient (Fig. 8a) and because of the role of soil water hydrology on chemical weathering with hydrological parameters, i.e., infiltration (I ; m³ yr⁻¹; Fig. 8b), average moisture content (θ ; m³ m⁻³; Fig. 8c), and water residence time (RT; year; Fig. 8d). The hydrological parameters were derived from the simulations. We also explored the relation with other variables, such as curvature and upslope contributing area (not shown in Fig. 8), but found no significant relation. This corroborates field measurements by Şensoy and Kara (2014) that have shown that the effect of curvature on runoff production is not clear.

The results indicated an absence of correlation with the current slope (Fig. 8a). Although the highest CDF values were found for two soil profiles with a low slope gradient (SC4 and SC7), this was not the case for SC10. On the other hand, the data indicate a positive relationship with average moisture content and infiltration. This implies that higher infiltration leads to higher chemical weathering. A negative relation was observed with residence time, implying that a faster throughflow of reactive water from rainfall speeds up the weathering process. The absence of statistically significant relations for slope and these hydrological parameters could be due to the complexity of the modelled processes or due to the geomorphology and landforms. One reason for this is the long timescale of modelling, and the current topography might not have been constant during the full period of weathering. The slope gradient is kept constant for the entire soil profile simulation time of 20 000 years as steady-state topography is assumed, following, for instance, Rempe and Dietrich (2014). This is a valid assumption in slowly eroding natural landscapes, although in 20 000 years the slope gradient of the sample points could have changed. This is a common problem in historical modelling of soil erosion in agricultural landscapes as the slope diminishes with time due to erosion and the flattening out of the landscapes. In such agricultural landscapes, the steady-state assumption is

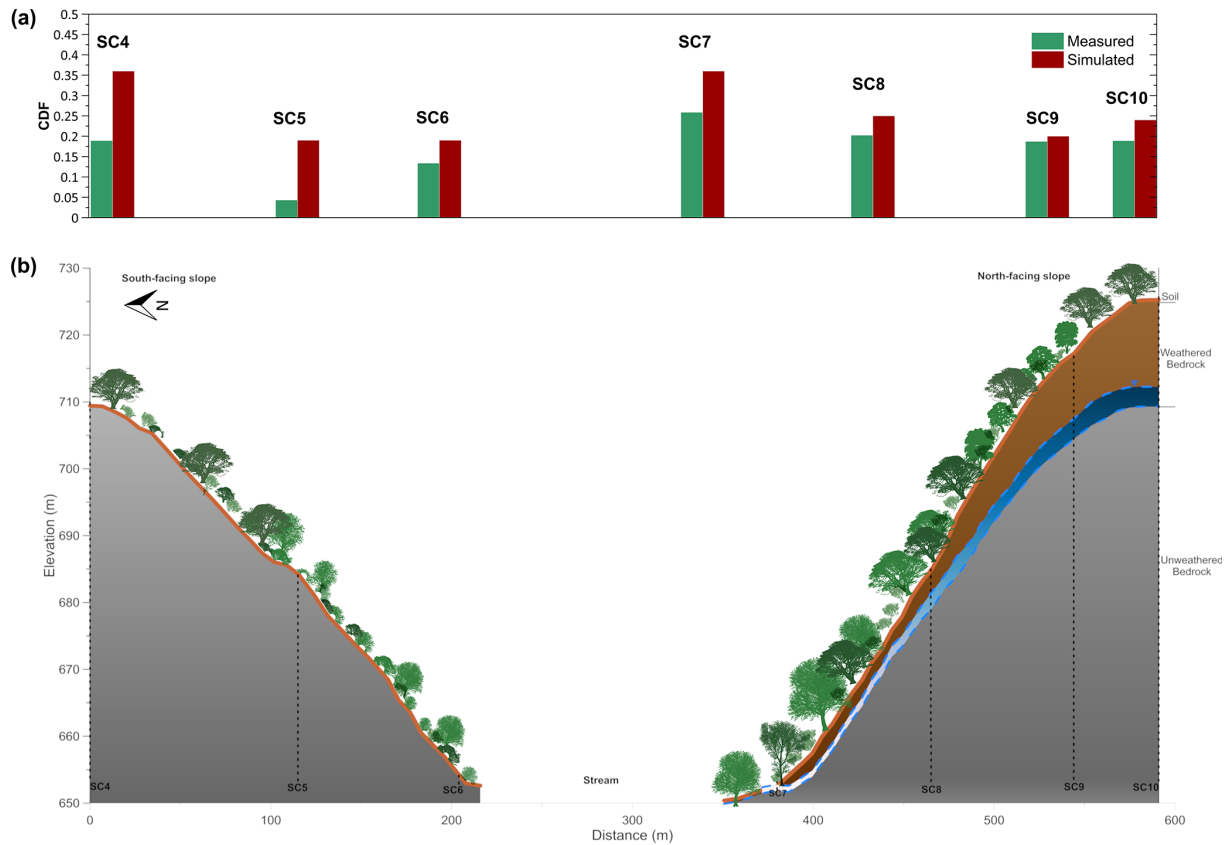


Figure 7. Variation in measured (green bars) and simulated (red bars) chemical depletion fraction (CDF) (a) along the studied north–south catena, including a schematic representation (b) of the vegetation, surface topography, soil, weathered bedrock, and unweathered bedrock. On the NFS, we also distinguish a seasonal groundwater table (blue).

Table 4. Bulk mineralogy along the catena, analysed by X-ray diffraction (XRD).

Location	Mineral composition				
	Quartz	Feldspar (plagioclase, orthoclase)	Mica (muscovite/ biotite/illite)	Chlorite– vermiculite	Kaolinite
SC4	X	X	X	X	X
SC5	X	X	(X)*	X	X
SC6	X	X	X	X	X
SC7	X	X	X	X	X
SC8	X	X	X	X	X
SC9	X	X	X	X	X
SC10	X	X	X	X	X

* At the SC5 location, the mica content was markedly lower compared to the other points (see Fig. S1 in the Supplement).

not valid, as erosion rates are quite high, but in any case, erosion is modelled using current topography because of a lack of a better alternative. Some authors (Peeters et al., 2006) attempted to develop backward modelling solutions, where the topography is iteratively rejuvenated by taking into account modelled erosion and deposition rates, but these mod-

els need detailed input data which is not usually available, and, at present, is not available in soil formation models.

The good relation between chemical weathering and hydrological variables corroborates previous studies that concluded the hydrological control on chemical weathering to be dominant (Lasaga et al., 1994; Maher, 2010; Maher and

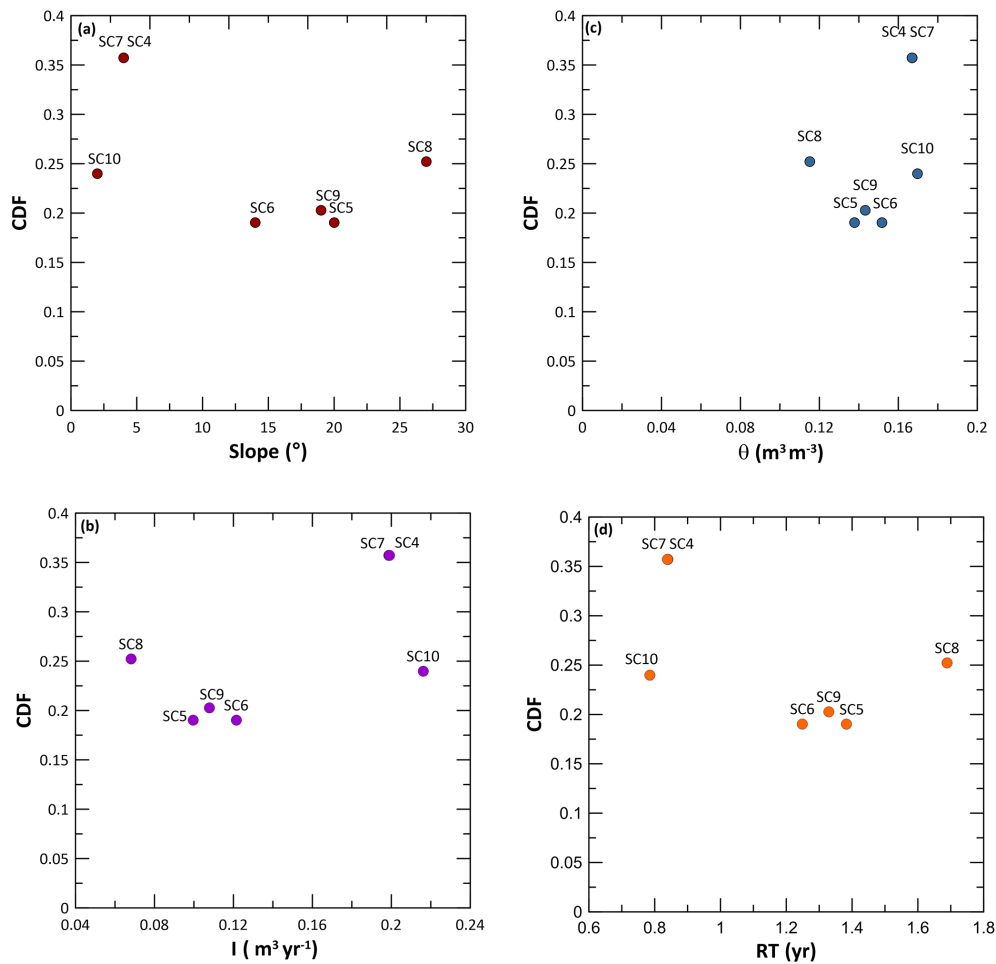


Figure 8. Relation between CDF values and the (a) local gradient slope ($^{\circ}$), (b) infiltration (I ; $\text{m}^3 \text{yr}^{-1}$), (c) average soil moisture (θ ; $\text{m}^3 \text{m}^{-3}$), and (d) water residence time (RT; year).

Chamberlain, 2014). It should be noted that this is well known already from early pedological research; for example, Jenny (1941) found a good correlation between carbonate precipitation and precipitation in loess soils in the USA. However, the quantification of specific weathering processes is new, and the recent studies quantifying the hydrological regulation of chemical weathering processes have important implications beyond soil formation, for example, on the geological carbon cycle (Maher and Chamberlain, 2014). Maher (2010) indicates that natural systems can generally be considered to be transport controlled, where the reaction rate of chemical weathering processes depends mostly on the departure from the equilibrium. This departure is controlled by the water flow rate through the profile and how fast or slow weathered products are exported from the soil profile. In other words, in transport-controlled weathering systems, flow rates and solubility by definition will be the dominant control on mass removal. As natural systems are difficult to characterize fully, not much field data have been collected to corroborate this so far. Some studies, like Schoonejans et

al. (2016), found a positive relation between chemical weathering and rainfall along a climatic gradient in southern Spain. However, the results of this study, both measured and modelled CDF values, are among the first to find differences in chemical weathering in different landscape positions along a catena. In this study area, rainfall is homogeneous, but the differences in infiltration can be purely attributed to differences in exposition and landscape position. Further studies will be needed, not only at the landscape or regional scale but also at a shorter spatial scale, such as this catena-scale study to elucidate these hydrological effects in more detail. Some authors have pointed to important feedbacks with plants that definitely can have a significant impact on soil hydrology and perhaps also a direct influence on chemical weathering processes (Cipolla et al., 2021; Porada et al., 2016).

The results of this study are in contrast with observations by Molina et al. (2019) on 10 toposequences in a high Andean catchment. They observed only a marginally significant topographic control on chemical weathering extent, while our data vary considerably between landscape posi-

tions. Rather than topography, Molina et al. (2019) concluded that vegetation exerted an important control, as they found highly significant differences in chemical weathering extent between vegetation communities. In their study, however, they compared very different vegetation types, ranging from forest to grass and cushion-forming plants. In our study, vegetation is more similar between SFS and NFS, although vegetation is denser on the latter. This could have an effect on acid supply but also on hydrology. Although counterintuitively, in previous work in the study site to characterize the hydrological dynamics using soil moisture sensors and piezometers, García-Gamero et al. (2021) observed very similar surface hydrological dynamics between the NFS and SFS. In fact, daily soil moisture storage change differences between both opposing slopes did not suggest more interception on the NFS (García-Gamero et al., 2021), despite the denser vegetation. The denser vegetation cover on the NFS only caused it to dry out somewhat earlier during the year compared to the SFS. However, subsurface water dynamics were found to be significantly different, with a deeper weathered bedrock on the NFS (Fig. 7) that allows seasonal water storage and a significant lateral water flow. A good correlation between the normalized difference vegetation index (NDVI) and the water table evolution was found on the NFS (García-Gamero et al., 2021).

The model SoilGen could be further improved by taking into account lateral fluxes of water and sediment. The one-dimensional SoilGen model does not consider lateral fluxes by definition. These lateral water fluxes on the NFS could explain the higher measured CDF values in SC9, SC8, and particularly in SC7. The points located along this NFS all receive an additional lateral water influx, which is greatest for SC7 at the toe slope. This lateral water flux can accelerate the chemical weathering and is not considered in the one-dimensional model. At present, as far as the authors know, no soil profile formation model exists that has this capability. On the other hand, on the SFS soils are shallower, and this lateral connectivity does not exist. The other profile on the SFS, SC6, however, does behave as expected and is characterized by the lowest CDF values, except for SC5 mentioned above, for both measured and simulated values. To take into account these lateral fluxes goes beyond the objectives of this paper that aims to model chemical weathering with a simple model, but future modelling efforts should be pointed in this direction.

3.3 Climatic effect on chemical weathering: sensitivity analysis

After analysing the variability in soil formation along the north–south-oriented catena, the effect of a simulated precipitation gradient (200–1200 mm) on the CDF was studied at one fixed, representative location, SC10 (Fig. 9).

The lowest CDF values throughout the profile correspond to the lowest precipitation value of 200 mm, as expected.

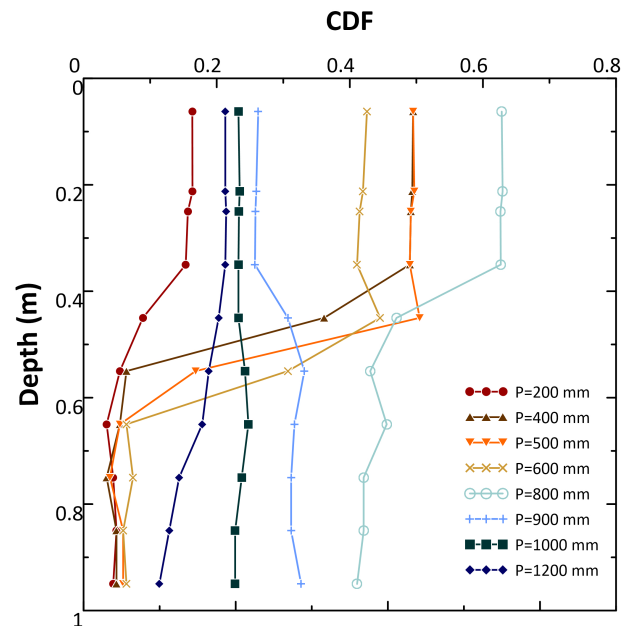


Figure 9. Weathering intensity (expressed by the chemical depletion fraction, CDF) of a soil profile under different annual rainfall (P). Profiles are simulated in the SC10 location at the summit.

For this precipitation value, there is very little difference in CDF with depth. Increasing precipitation to 400 mm leads to a sudden increase in the weathering of the top 40 cm of the profile, with a marked depth gradient and similar CDF values in depth compared to the 200 mm case. A precipitation increase to 600 mm does not change the CDF depth pattern much, although the weathering front lowers. In the situation with low precipitation ($P = 200\text{--}600\text{ mm yr}^{-1}$), the rainfall is lower than the potential evapotranspiration, and as a consequence, only the upper 45 cm of the profile are wetted while the lower part remains dry. This means that the contact time of meteoric water with the topsoil is long while it is near zero in the subsoil. A long contact time allows for more weathering, and this is reflected by higher CDF in the topsoil than in the subsoil. This contrast increases with precipitation increasing from 200 to 600 mm, as mentioned above. At $P = 800\text{ mm yr}^{-1}$ the weathering and CDF values in depth increase markedly, the lower part of the profile also is moistened and the contrast decreases, while the contact time is still large, resulting in a high CDF. These simulated depth patterns are comparable to those measured in the eastern part of the Betic cordillera, where precipitation ranges between 275–425 mm, as located in southeastern Spain by Schoonejans et al. (2016). However, at even higher precipitation, $P > 800\text{ mm yr}^{-1}$, the subsoil is moistened, and this increases the hydraulic conductivity and thus decreases the contact time. As a result, the CDF decrease and also the topsoil–subsoil contrast in CDF disappears (Fig. 9). The latter simulated depth patterns are comparable to those measured by Oeser and von Blanckenburg (2020) in their study,

mentioned above, in an arid to humid climate and vegetation gradient in the Chilean coastal cordillera. These authors found that the average CDF for the profile (combined analysis of NFS and SFS profiles) amounts to 0.25 in the humid temperate site in granitic rock (granodiorite), with a mean annual precipitation of 1084 mm. This value is similar to that simulated for precipitation of 1000 mm in our work (Fig. 9).

Figure 10 then shows the total CDF, averaged over the entire soil depth, i.e., 1 m of the soil profile. The results from this study, represented by the blue dots, showed an increased weathering up to 800 mm, but after this critical value, the profiles were less weathered. Moreover, in Fig. 10, the CDFs of this study are compared to a global data compilation of granitic soil-mantled hillslopes (Schaller and Ehlers, 2022). Also, this global dataset seems to indicate that high weathering rates measured as CDF are not obtained with the highest precipitation values but rather with intermediate precipitation. With precipitation less than 800 mm, a substantial part of the year will have a precipitation deficit. This means that leaching is of less importance and concentrations of cations released by weathering in the soil solution will be high. One theory often applied to quantify weathering is the transition state theory (TST). In the quantification of weathering fluxes by TST, the dissolution rate of a mineral is the product of the rate parameter (which is often a function of pH) and the degree of saturation of the soil solution with respect to the dissolving mineral. Drier climates often result in a higher pH and a higher degree of saturation, which both (and certainly in combination) lead to lower weathering rates for most minerals. The decreasing weathering rates imply decreasing CDF values with lower precipitation. The lower the precipitation, the higher the deficit, leading to a high CDF in only that part of the soil that becomes moistened because the contact time is large (no leaching). The lower the precipitation, the thinner the part that is moistened, and thus the lower the profile of the average CDF. At higher precipitation up till 800 mm, the moistened part of the soil profile becomes thicker and thus increases the profile of the average CDF. This is the upward branch of the Albrecht curve.

At still higher precipitation, the whole soil becomes moist, with higher hydraulic conductivity and increasing water flow velocities throughout and, hence, lower contact time and decreasing CDF. Thus, the downward branch of the curve represents a situation of increased leaching but, at the same time, less intensive weathering because the contact time decreases.

Additionally, vegetation will be more lush, and then the nutrient pump may prevent the leaching of some elements. Both will decrease the CDF.

This threshold or maximum weathering correspondent to intermediate precipitation is coincident with the maximum generalization of Albrecht's curve, which is shown in Fig. 10 by the grey shaded area. Huston (2012) pointed out the link between climate and soil formation and properties that scientists such as William Albrecht generalized 80 years ago. Albrecht's curve (e.g. Albrecht, 1957) is a rule that illus-

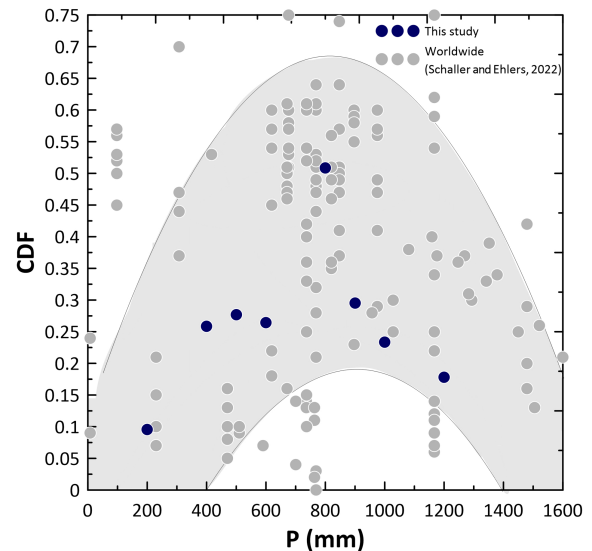


Figure 10. Chemical weathering (CDF) versus annual precipitation. The expected trend is indicated by the shaded area and follows a parabolic pattern with maximum chemical weathering for intermediate precipitation. Observations from this study are depth averaged (blue dots). Observations from other study sites situated in granitic soil-mantled hillslopes (grey dots) are from a review by Schaller and Ehlers (2022).

trated the effect of precipitation on soil-forming processes and soil properties (Huston, 2012). In this diagram, which presents a maximum in the centre, the effect of a precipitation gradient on the rates of physical, chemical, and biological processes that affect pedogenesis and important soil properties are shown. Different later works that have studied soil properties and weathering along a marked precipitation gradient (e.g. Chadwick et al., 2003) confirmed Albrecht's curve. Similarly, Dixon et al. (2016), in their study for chemical weathering in postglacial soils of New Zealand, found an important pedogenic threshold coincident at a mean annual precipitation of $\sim 800 \text{ mm yr}^{-1}$, which is very similar to the threshold value that was identified in this sensitivity analysis. Oeser and von Blanckenburg (2020) on the other hand, in their study in the EarthShape Critical Zone located along the Chilean coastal cordillera, found no correlation between the degree of weathering and mean annual precipitation. Therefore, they pointed out that a competitive effect seems to offset the expected increase in the rate of weathering with precipitation. Huston (2012) even related this concept of the Albrecht curve to ecosystem trends. He analysed global variations in soil properties, net primary productivity, and biodiversity as a function of precipitation. He found similar, unimodal curves with maximum values for soil properties, such as total exchangeable bases, and found that the maximum corresponded to the point where precipitation is equal to the evapotranspiration rate. Given the importance of soil properties and the chemical weathering of soil profiles

for ecosystem response, these results can have far-reaching consequences and should be explored further with more simulations and profile data.

4 Conclusions

The effect of topographic position and hydrology on chemical weathering was analysed in soils formed on granites under a Mediterranean climate. The chemical depletion fraction was measured and modelled in seven locations selected along a north–south-oriented catena in southern Spain. The model SoilGen was used to simulate pedogenesis and the measured chemical weathering status over a 20 000-year period.

Despite the complexity of the catena and the hydrological conditions, a good correspondence was obtained between modelled and measured CDF. The variability in CDF values was explained better by hydrological variables than by topography. No clear relation to the catena position was found. No relation with the slope gradient was observed. However, the CDF data did indicate a positive relation to the hydrological variables of soil moisture and infiltration, and a negative relation to water residence time. In addition, differences between measured and simulated CDF values could be attributed to lateral water fluxes that are not considered in the model.

The model sensitivity was evaluated with different precipitation regimes. The results showed a marked depth gradient for rainfall under 800 mm for the CDF, but it showed a uniform depth distribution for precipitation above 800 mm. For the profile average chemical weathering, maximum values were observed for intermediate precipitation values, at around 800 mm.

Data availability. Data are available upon request to the authors.

Supplement. The supplement related to this article is available online at: <https://doi.org/10.5194/soil-8-319-2022-supplement>.

Author contributions. TV and VGG conceived and designed the study, with substantial input from PAF and AP. ARS and TV performed the sampling. The data curation and formal analysis, methodology, and visualization for the paper were performed by VGG, with substantial input from PAF and TV. VGG and PAF performed the simulations. VGG wrote the first draft. All the authors (VGG, TV, AP, ARS, and PAF) contributed to generating and reviewing the subsequent versions of the paper.

Competing interests. At least one of the (co-)authors is a member of the editorial board of *SOIL*. The peer-review process was guided by an independent editor, and the authors also have no other competing interests to declare.

Disclaimer. Publisher’s note: Copernicus Publications remains neutral with regard to jurisdictional claims in published maps and institutional affiliations.

Acknowledgements. This work has been supported by the project “Estableciendo un Observatorio de la Zona Crítica para la Hidropedología y Agricultura Sostenible en el Mediterráneo” (grant no. AGL2015-65036-C3-2-R) funded by Programa Estatal de Investigación, Desarrollo e Innovación orientada a los retos de la sociedad 81/150 para el cuatrienio 2016–2020 (MINECO/FEDER, UE). Vanesa García-Gamero was awarded a FPU fellowship (grant no. FPU15/05279) from the Spanish Ministry of Education, Culture, and Sport. This paper was the result of a research stay by Vanesa García-Gamero at Ghent University, funded by the fellowship “Becas Movilidad Internacional” (2017–2018) from Universidad de Córdoba.

Tom Vanwalleghem is thankful for the funding from the Department of Agronomy, of the Spanish Ministry of Science and Innovation, and the Spanish State Research Agency, through the Severo Ochoa and María de Maeztu Program for Centres and Units of Excellence in R and D (grant no. CEX2019-000968-M).

Financial support. This research has been supported by the Ministerio de Economía, Industria y Competitividad, Gobierno de España (grant no. AGL2015-65036-C3-2-R), the Ministerio de Educación, Cultura y Deporte (grant no. FPU15/05279), and the Ministerio de Ciencia e Innovación (grant no. CEX2019-000968-M).

Review statement. This paper was edited by Jeffrey Homburg and reviewed by three anonymous referees.

References

- Albrecht, W. A.: Soil Fertility and Biotic Geography, *Geogr. Rev.*, 47, 86, 47, 86–105, <https://doi.org/10.2307/212191>, 1957.
- Borden, R. W., Baillie, I. C., and Hallett, S. H.: The East African contribution to the formalisation of the soil catena concept, *Catena*, 185, 104291, <https://doi.org/10.1016/j.catena.2019.104291>, 2020.
- Boylan, J. W. and Russell, A. G.: PM and light extinction model performance metrics, goals, and criteria for three-dimensional air quality models, *Atmos. Environ.*, 40, 4946–4959, <https://doi.org/10.1016/j.atmosenv.2005.09.087>, 2006.
- Brancher, M., Hieden, A., Baumann-Stanzer, K., Schaubberger, G., and Piringer, M.: Performance evaluation of approaches to predict sub-hourly peak odour concentrations, *Atmos. Environ.*, 7, 100076, <https://doi.org/10.1016/j.aeaoa.2020.100076>, 2020.
- Brantley, S. L., Lebedeva, M. I., Balashov, V. N., Singha, K., Sullivan, P. L., and Stinchcomb, G.: Toward a conceptual model relating chemical reaction fronts to water flow paths in hills, *Geomorphology*, 277, 100–117, <https://doi.org/10.1016/j.geomorph.2016.09.027>, 2017.
- Braun, J., Mercier, J., Guillocheau, F., and Robin, C.: A simple model for regolith formation by chemical

- weathering, *J. Geophys. Res.-Earth*, 121, 2140–2171, <https://doi.org/10.1002/2016JF003914>, 2016.
- Calabrese, S. and Porporato, A.: Wetness controls on global chemical weathering, *Environ. Res. Commun.*, 2, 085005, <https://doi.org/10.1088/2515-7620/abad7b>, 2020.
- Carpintero, E., Andreu, A., Gómez-Giráldez, P. J., Blázquez, Á., and González-Dugo, M. P.: Remote-Sensing-Based Water Balance for Monitoring of Evapotranspiration and Water Stress of a Mediterranean Oak – Grass Savanna, *Water*, 12, 1418, <https://doi.org/10.3390/w12051418>, 2020.
- Carracedo, M., Paquette, J. L., Alonso Olazabal, A., Santos Zalduogui, J. F., de García de Madinabeitia, S., Tiepolo, M., and Gil Ibarguchi, J. I.: U-Pb dating of granodiorite and granite units of the Los Pedroches batholith. Implications for geodynamic models of the southern Central Iberian Zone (Iberian Massif), *Int. J. Earth Sci.*, 98, 1609–1624, <https://doi.org/10.1007/s00531-008-0317-0>, 2009.
- Chadwick, O. A., Gavenda, R. T., Kelly, E. F., Ziegler, K., Olson, C. G., Crawford Elliott, W., and Hendricks, D. M.: The impact of climate on the biogeochemical functioning of volcanic soils, *Chem. Geol.*, 202, 195–223, <https://doi.org/10.1016/j.chemgeo.2002.09.001>, 2003.
- Chadwick, O. A., Roering, J. J., Heimsath, A. M., Levick, S. R., Asner, G. P., and Khomo, L.: Shaping post-orogenic landscapes by climate and chemical weathering, *Geology*, 41, 1171–1174, <https://doi.org/10.1130/G34721.1>, 2013.
- Cipolla, G., Calabrese, S., Valerio, L., and Porporato, A.: The role of hydrology on enhanced weathering for carbon sequestration I. Modeling rock-dissolution reactions coupled to plant, soil moisture, and carbon dynamics, *Adv. Water Resour.*, 154, 103934, <https://doi.org/10.1016/j.advwatres.2021.103934>, 2021.
- Cohen, S., Willgoose, G., and Hancock, G.: The mARM3D spatially distributed soil evolution model: Three-dimensional model framework and analysis of hillslope and landform responses, *J. Geophys. Res.-Earth*, 115, 1–16, <https://doi.org/10.1029/2009JF001536>, 2010.
- Coleman, K. and Jenkinson, D.: RothC-26.3 - A Model for the turnover of carbon in soil, *Eval. Soil Org. Matter Model.*, 38, 237–246, https://doi.org/10.1007/978-3-642-61094-3_17, 1996.
- Dahlgren, R. A., Boettinger, J. L., Huntington, G. L., and Amundson, R. G.: Soil development along an elevational transect in the western Sierra Nevada, California, *Geoderma*, 78, 207–236, [https://doi.org/10.1016/S0016-7061\(97\)00034-7](https://doi.org/10.1016/S0016-7061(97)00034-7), 1997.
- Davis, B. A. S., Brewer, S., Stevenson, A. C., Guiot, J. and Data contributors: The temperature of Europe during the Holocene reconstructed from pollen data, *Quaternary Sci. Rev.*, 22, 1701–1716, [https://doi.org/10.1016/S0277-3791\(03\)00173-2](https://doi.org/10.1016/S0277-3791(03)00173-2), 2003.
- De Vries, W. and Posch, M.: Derivation of cation exchange constants for sand loess, clay and peat soils on the basis of field measurements in the Netherlands, *Alterra-Report 701*, Alterra Green World Research, Wageningen, 50 pp., ISSN: 1566-7197, 2003.
- Dixon, J., Heimsath, A. M., and Amundson, R.: The critical role of climate and saprolite weathering in landscape evolution, *Earth Surf. Process. Land.*, 34, 1507–1521, <https://doi.org/10.1002/esp.1836>, 2009.
- Dixon, J. L., Chadwick, O. A., and Vitousek, P. M.: Climate-driven thresholds for chemical weathering in postglacial soils of New Zealand, *J. Geophys. Res.-Earth*, 121, 1619–1634, <https://doi.org/10.1002/2016JF003864>, 2016.
- Dong, X., Cohen, M. J., Martin, J. B., McLaughlin, D. L., Murray, A. B., Ward, N. D., Flint, M. K., and Heffernan, J. B.: Ecohydrologic processes and soil thickness feedbacks control limestone-weathering rates in a karst landscape, *Chem. Geol.*, 527, 118774, <https://doi.org/10.1016/J.CHEMGEO.2018.05.021>, 2019.
- Duarte, I. M. R., Gomes, C. S. F., and Pinho, A. B.: Chemical Weathering, in: *Encyclopedia of Engineering Geology*. *Encyclopedia of Earth Sciences Series*, edited by: Bobrowsky, P. T. and Marker, B., Springer, Cham, https://doi.org/10.1007/978-3-319-12127-7_49-1, 2017.
- Ferrier, K. L. and Perron, J. T.: The importance of hillslope scale in responses of chemical erosion rate to changes in tectonics and climate, *J. Geophys. Res. Earth Surf.*, 125, e2020JF005562, <https://doi.org/10.1029/2020JF005562>, 2020.
- Finke, P. A.: Modeling the genesis of luvisols as a function of topographic position in loess parent material, *Quaternary Int.*, 265, 3–17, <https://doi.org/10.1016/j.quaint.2011.10.016>, 2012.
- Finke, P. A. and Hutson, J. L.: Modelling soil genesis in calcareous loess, *Geoderma*, 145, 462–479, <https://doi.org/10.1016/j.geoderma.2008.01.017>, 2008.
- Finke, P. A., Vanwalleghem, T., Opolot, E., Poesen, J., and Deckers, J.: Estimating the effect of tree uprooting on variation of soil horizon depth by confronting pedogenetic simulations to measurements in a Belgian loess area, *J. Geophys. Res.-Earth*, 118, 2124–2139, <https://doi.org/10.1002/jgrf.20153>, 2013.
- Gabet, E. J. and Mudd, S. M.: A theoretical model coupling chemical weathering rates with denudation rates, *Geology*, 37, 151–154, <https://doi.org/10.1130/G25270A.1>, 2009.
- García-Gamero, V., Peña, A., Laguna, A. M., Giráldez, J. V., and Vanwalleghem, T.: Factors controlling the asymmetry of soil moisture and vegetation dynamics in a hilly mediterranean catchment, *J. Hydrol.*, 598, 126207, <https://doi.org/10.1016/j.jhydrol.2021.126207>, 2021.
- Gobat, J.-M., Aragno, M., and Matthey, W.: *Le Sol Vivant*, Les Presses polytechniques et universitaires romandes, Lausanne, Presses polytechniques et universitaires romandes, ISBN: 978-2-88074-718-3, 1998.
- Hargreaves, G. H. and Samani, Z. A.: Reference Crop Evapotranspiration from Temperature, *Appl. Eng. Agric.*, 1, 96–99, 1985.
- Huston, M. A.: Precipitation, soils, NPP, and biodiversity: Resurrection of Albrecht's curve, *Ecol. Monogr.*, 82, 277–296, <https://doi.org/10.1890/11-1927.1>, 2012.
- IUSS Working Group WRB: World reference base for soil resources 2014, update 2015 International soil classification system for naming soils and creating legends for soil maps, FAO, Roma, Food and Agricultural Organization of the United Nations, ISBN: 978-92-5-108369-7, 2015.
- Jenny, H.: *Factors of soil formation: A System of Quantitative Pedology*, McGraw-Hill Book Company Inc., New York, McGraw-Hill Book Company Inc., ISBN: 0-486-68128-9, 1941.
- Kontos, S., Kakosimos, K., Liora, N., Poupkou, A., and Melas, D.: Towards a regional dust modeling system in the central Middle East: Evaluation, uncertainties and recommendations, *Atmos. Environ.*, 246, 118160, <https://doi.org/10.1016/j.atmosenv.2020.118160>, 2021.
- Kumar, A., Luo, J., and Bennett, G. F.: Statistical evaluation of Lower Flammability Distance (LFD) using four hazardous release models, *Process. Saf. Prog.*, 12, 1–11, <https://doi.org/10.1002/prs.680120103>, 1993.

- Lachassagne, P. and Wyns, R.: Review article The fracture permeability of Hard Rock Aquifers is due neither to tectonics, nor to unloading, but to weathering processes, *Terra Nov.*, 23, 145–161, <https://doi.org/10.1111/j.1365-3121.2011.00998.x>, 2011.
- Laio, F., Porporato, A., Ridolfi, L., and Rodriguez-Iturbe, I.: Plants in water-controlled ecosystems: active role in hydrologic processes and response to water stress. II. Probabilistic soil moisture dynamics., *Adv. Water Resour.*, 24, 707–723, 2001.
- Langston, A. L., Tucker, G. E., Anderson, R. S., and Anderson, S. P.: Exploring links between vadose zone hydrology and chemical weathering in the Boulder Creek critical zone observatory, *Appl. Geochem.*, 26, S70–S71, <https://doi.org/10.1016/j.apgeochem.2011.03.033>, 2011.
- Larsen, I. J., Almond, P. C., Eger, A., Stone, J. O., Montgomery, D. R., and Malcolm, B.: Rapid Soil Production and Weathering in the Southern Alps, New Zealand, *Science*, 343, 637–640, <https://doi.org/10.1126/science.1244908>, 2014.
- Lasaga, A. C., Soler, J. M., Ganor, J., Burch, T. E., and Nagy, K. L.: Chemical weathering rate laws and global geochemical cycles, *Geochim. Cosmochim. Ac.*, 58, 2361–2386, [https://doi.org/10.1016/0016-7037\(94\)90016-7](https://doi.org/10.1016/0016-7037(94)90016-7), 1994.
- Lebedeva, M. I. and Brantley, S. L.: Relating the depth of the water table to depth of weathering, *Earth Surf. Process. Land.*, 45, 2167–2178, <https://doi.org/10.1002/esp.4873>, 2020.
- Maher, K.: The dependence of chemical weathering rates on fluid residence time, *Earth Planet. Sc. Lett.*, 294, 101–110, <https://doi.org/10.1016/j.epsl.2010.03.010>, 2010.
- Maher, K.: The role of fluid residence time and topographic scales in determining chemical fluxes from landscapes, *Earth Planet. Sc. Lett.*, 312, 48–58, <https://doi.org/10.1016/j.epsl.2011.09.040>, 2011.
- Maher, K. and Chamberlain, C. P.: Hydrologic Regulation of Chemical, *Science*, 1502, <https://doi.org/10.1126/science.1250770>, 2014.
- Milne, G.: Some suggested units of classification and mapping particularly for East African soils, *Soil Res., Suppl. to Proc. Int. Union Soil Sci. IV*, 183–198, 1935.
- Minasny, B. and McBratney, A. B.: A rudimentary mechanistic model for soil formation and landscape development II, A two-dimensional model incorporating chemical weathering, *Geoderma*, 103, 161–179, [https://doi.org/10.1016/S0016-7061\(01\)00075-1](https://doi.org/10.1016/S0016-7061(01)00075-1), 2001.
- Molina, A., Vanacker, V., Corre, M. D., and Veldkamp, E.: Patterns in Soil Chemical Weathering Related to Topographic Gradients and Vegetation Structure in a High Andean Tropical Ecosystem, *J. Geophys. Res.-Earth*, 124, 666–685, <https://doi.org/10.1029/2018JF004856>, 2019.
- Mudd, S. M. and Furbish, D. J.: Using chemical tracers in hillslope soils to estimate the importance of chemical denudation under conditions of downslope sediment transport, *J. Geophys. Res.-Earth*, 111, F02021, <https://doi.org/10.1029/2005JF000343>, 2006.
- Oeser, R. A. and Von Blanckenburg, F.: Do degree and rate of silicate weathering depend on plant productivity?, *Biogeosciences*, 17, 4883–4917, <https://doi.org/10.5194/bg-17-4883-2020>, 2020.
- Olea, L. and San Miguel-Ayanz, A.: The Spanish dehesa, a traditional Mediterranean silvopastoral system linking production and nature conservation, in: 21st General meeting of the European Grassland Federation, Badajoz, Spain, 3–6 April 2006, Opening paper, 3–13, ISBN: 84 689 6711 4, 2006.
- Opolot, E. and Finke, P. A.: Evaluating sensitivity of silicate mineral dissolution rates to physical weathering using a soil evolution model (SoilGen2.25), *Biogeosciences*, 12, 6791–6808, <https://doi.org/10.5194/bg-12-6791-2015>, 2015.
- Opolot, E., Yu, Y. Y., and Finke, P. A.: Modeling soil genesis at pedon and landscape scales: Achievements and problems, *Quaternary Int.*, 376, 34–46, <https://doi.org/10.1016/j.quaint.2014.02.017>, 2015.
- Peel, M. C., Finlayson, B. L., and McMahon, T. A.: Updated world map of the Köppen-Geiger climate classification, *Hydrol. Earth Syst. Sci.*, 11, 1633–1644, <https://doi.org/10.5194/hess-11-1633-2007>, 2007.
- Peeters, I., Rommens, T., Verstraeten, G., Govers, G., Van Rompaey, A., Poesen, J., and Van Oost, K.: Reconstructing ancient topography through erosion modelling, *Geomorphology*, 78, 250–264, <https://doi.org/10.1016/j.geomorph.2006.01.033>, 2006.
- Porada, P., Lenton, T. M., Pohl, A., Weber, B., Mander, L., Donnadieu, Y., Beer, C., Po, U., and Kleidon, A.: High potential for weathering and climate effects of non-vascular vegetation in the Late Ordovician, *Nat. Commun.*, 7, 12113, <https://doi.org/10.1038/ncomms12113>, 2016.
- Rempe, D. M. and Dietrich, W. E.: A bottom-up control on fresh-bedrock topography under landscapes, *P. Natl. Acad. Sci. USA*, 111, 6576–6581, <https://doi.org/10.1073/pnas.1404763111>, 2014.
- Reuter, R. J. and Bell, J. C.: Soils and Hydrology of a Wet-Sandy Catena in East-Central Minnesota, *Soil Sci. Soc. Am. J.*, 65, 1559–1569, <https://doi.org/10.2136/sssaj2001.6551559x>, 2001.
- Riebe, C. S., Kirchner, J. W., Granger, D. E., and Finkel, R. C.: Strong tectonic and weak climatic control of long-term chemical weathering rates, *Geol. Soc. Am.*, 29, 511–514, 2001.
- Riebe, C. S., Kirchner, J. W., and Finkel, R. C.: Erosional and climatic effects on long-term chemical weathering rates in granitic landscapes spanning diverse climate regimes, *Earth Planet. Sc. Lett.*, 224, 547–562, <https://doi.org/10.1016/j.epsl.2004.05.019>, 2004.
- Román-Sánchez, A., Vanwalleghem, T., Peña, A., Laguna, A., and Giráldez, J. V.: Controls on soil carbon storage from topography and vegetation in a rocky, semi-arid landscapes, *Geoderma*, 311, 159–166, <https://doi.org/10.1016/j.geoderma.2016.10.013>, 2018.
- Román-Sánchez, A., Reimann, T., Wallinga, J., and Vanwalleghem, T.: Bioturbation and erosion rates along the soil-hillslope conveyor belt, part 1: Insights from single-grain feldspar luminescence, *Earth Surf. Process. Land.*, 44, 2051–2065, <https://doi.org/10.1002/esp.4628>, 2019.
- Salve, R., Rempe, D. M., and Dietrich, W. E.: Rain, rock moisture dynamics, and the rapid response of perched groundwater in weathered, fractured argillite underlying a steep hillslope, *Water Resour. Res.*, 48, 1–25, <https://doi.org/10.1029/2012WR012583>, 2012.
- Samouëlian, A. and Cornu, S.: Modelling the formation and evolution of soils, towards an initial synthesis, *Geoderma*, 145, 401–409, <https://doi.org/10.1016/j.geoderma.2008.01.016>, 2008.
- Schaetzl, R. J. and Anderson, S.: *Soils: Genesis and Geomorphology*, Cambridge University Press, ISBN: 978-0521812016, 2005.

- Schaller, M. and Ehlers, T. A.: Comparison of soil production, chemical weathering, and physical erosion rates along a climate and ecological gradient (Chile) to global observations, *Earth Surf. Dynam.*, 10, 131–150, <https://doi.org/10.5194/esurf-10-131-2022>, 2022.
- Schoonejans, J., Vanacker, V., Opfergelt, S., Ameijeiras-Mariño, Y., and Christl, M.: Kinetically limited weathering at low denudation rates in semiarid climatic conditions, *J. Geophys. Res.-Earth*, 121, 336–350, <https://doi.org/10.1002/2015JF003626>, 2016.
- Şensoy, H. and Kara, Ö.: Slope shape effect on runoff and soil erosion under natural rainfall conditions, *iForest-Bioge. For.*, 7, 110–114, <https://doi.org/10.3832/IFOR0845-007>, 2014.
- Temme, A. J. A. M. and Vanwallegghem, T.: LORICA – A new model for linking landscape and soil profile evolution: Development and sensitivity analysis, *Comput. Geosci.*, 90, 131–143, <https://doi.org/10.1016/j.cageo.2015.08.004>, 2016.
- Vanwallegghem, T., Stockmann, U., Minasny, B., and McBratney, A. B.: A quantitative model for integrating landscape evolution and soil formation, *J. Geophys. Res.-Earth*, 118, 331–347, <https://doi.org/10.1029/2011JF002296>, 2013.
- Welivitiya, W. D. D. P., Willgoose, G. R., and Hancock, G. R.: A coupled soilscape-landform evolution model: Model formulation and initial results, *Earth Surf. Dynam.*, 7, 591–607, <https://doi.org/10.5194/esurf-7-591-2019>, 2019.
- Whittig, L. D. and Allardice, W. R.: X-Ray Diffraction Techniques, in: *Methods of Soil Analysis, Part 1: Physical and Mineralogical Methods*, edited by: Klute, A., American Society of Agronomy, Madison, Soil Science Society of America, Inc., 331–362, ISBN: 9780891180883, 1986.
- Yoo, K., Amundson, R., Heimsath, A. M., Dietrich, W. E., and Brimhall, G. H.: Integration of geochemical mass balance with sediment transport to calculate rates of soil chemical weathering and transport on hillslopes, *J. Geophys. Res.*, 112, F02013, <https://doi.org/10.1029/2005JF000402>, 2007.
- Yoo, K., Mudd, S. M., Sanderman, J., Amundson, R., and Blum, A.: Spatial patterns and controls of soil chemical weathering rates along a transient hillslope, *Earth Planet. Sc. Lett.*, 288, 184–193, <https://doi.org/10.1016/j.epsl.2009.09.021>, 2009.
- Yoo, K., Weinman, B., Mudd, S. M., Hurst, M., Attal, M., and Maher, K.: Evolution of hillslope soils: The geomorphic theater and the geochemical play, *Appl. Geochem.*, 26, 149–153, <https://doi.org/10.1016/j.apgeochem.2011.03.054>, 2011.